Rapid Synthesis of MFI Zeolite Nanocrystals

ARTICLE *in* THE JOURNAL OF PHYSICAL CHEMISTRY B · NOVEMBER 2005

Impact Factor: 3.3 · DOI: 10.1021/jp0526391 · Source: PubMed

Rapid Synthesis of MFI Zeolite Nanocrystals

Cheng-Ye Hsu,[†] Anthony S. T. Chiang,*[,†] Rosilda Selvin,[†] and Robert W. Thompson[‡]

Department of Chemical & Materials Engineering, National Central University, 300 JungDa Rd., Chung Li, Taiwan ROC 32054, and Department of Chemical Engineering, Worcester Polytechnic Institute, Worcester, Massachusetts 01609

Received: May 20, 2005; In Final Form: August 1, 2005

A rapid synthesis procedure for nonagglomerated silicalite nanocrystals has been developed. This was achieved by concentrating the precursor sol before 10−12 h of aging at 80 °C, followed by hydrothermal synthesis at 175 °C for 90 min. The high silica concentration in the concentrated sol accelerated the aggregation of primary units that were present early in the system. Thus, little silica nutrients were left for growth when the secondary particles were converted to zeolite during hydrothermal reaction. As a result, fully dispersible nanocrystals were obtained within a day instead of weeks as reported previously. The aggregation of primary units during the 80 °C aging process as well as the conversion of these aggregates into zeolite has been followed by DLS, XRD, and FTIR. In light of the new results, the nucleation and growth mechanisms of MFI zeolite that have been under debate in the literature were reexamined.

Introduction

Zeolites are microporous crystalline materials, routinely used as catalysts, ion-exchangers, and adsorbents. They were only available in the form of micrometer-sized crystals before the development of colloidal zeolite syntheses in the early 1990s.[1,2] Having zeolite nanocrystals smaller than 100 nm in the form of stable colloidal suspensions was a major event of the past decade in zeolite science. Since then, worldwide efforts have been devoted to the synthesis of nanocrystalline zeolites because of their technological importance. An extended review of the synthesis, crystallization mechanism, and application of colloidal zeolites was given by Tocheva and Valtchev[3] recently.

Compared to micrometer-sized zeolites, nanocrystalline zeolites have a larger external surface and a better accessibility to the internal micropores, properties that may be advantageous in some catalysis and adsorption applications. For example, catalyst deactivation has been shown to proceed slower in smaller crystals due to their shorter diffusion path.[4] The diffusion-limited partial oxidation of 2-butanol to 2-butanone is 3 times faster on 80 nm TS-1 nanocrystals than 560 nm crystallites.[5] Because of the larger external surface area, silicalite-1 nanocrystals showed a 50% increase in toluene adsorption capacity compared to the micrometer-sized counterpart.[6] In addition to these examples, zeolite nanocrystals may also find applications in areas such as sensors,[7] separation membranes,[8,9] and ultralow-*k* materials[10] for next generation electronics.

Many zeolites can be prepared in the form of colloidal suspensions with narrow particle size distributions, but the pure-silica MFI (silicalite-1) system is the most frequently studied. The synthesis of colloidal silicalite typically starts with a clear sol prepared from the hydrolysis of TEOS in TPAOH solution. Colloidal zeolites of about 90 nm in size can be produced from such a clear sol by direct heating at 98−115 °C for 2−3 days as done in the early work of Persson et al.[11,12] and our more recent work.[13]

It was learned later that zeolite growth is a more sensitive activated process than nucleation.[14,15] At low temperature, nucleation proceeds while growth is suppressed, leading to smaller crystals. To produce nanocrystals smaller than 60 nm, the synthesis solution can be aged at low temperatures (typically <60 °C) for several days before an optional hydrothermal treatment at a higher temperature.[16−21] Such a two-stage varying-temperature synthesis procedure was first proposed by Li et al.[18] and was shown to produce ∼60 nm nanocrystals within 7 days (aging 6 days at 60 °C and then raising to 100 °C for 1 day). Following the same logic, Mintova et al.[19] synthesized ∼30 nm silicalite nanocrystals by aging at room temperature for 30 days before heating to 90 °C for a few hours. However, the crystalline yields in these two studies were rather low, at about 50%. As demonstrated by Cundy et al.,[20] the crystalline yield could be increased to >75% without much increase of the crystal size if a higher temperature (175 °C) was employed after aging at room temperature for a very long time. Nevertheless, growth of the MFI crystals became excessive when the second stage temperature was further increased. For example, the crystal size increased to 260 nm when a precursor aged for 45 days was heated at 230 °C.[21]

In all of the above-cited works, days or even weeks were needed to synthesize silicalite nanocrystals, where by the term "synthesis" we refer to the combined processes of the aging and the high-temperature hydrothermal treatment steps. This is very counterintuitive, as one would expect the growth time required for smaller crystals to be shorter. The true difficulty, however, is to increase the number of nuclei and to suppress their growth. To increase the nucleation rate, the conventional wisdom suggests the use of higher supersaturation conditions, that is, by using a lower water/silica ratio.

The effect of the water/silica ratio in these "clear" solution silicalite syntheses has been reported previously.[11,13] For

[†] National Central University.
[‡] Worcester Polytechnic Institute.
* Corresponding author: Tel (+886) 3-4229274; e-mail stchiang@cc.ncu.edu.tw.

10.1021/jp0526391 CCC: $30.25
Published on Web 09/08/2005

example, in our earlier work on colloidal silicalite,[13] we found that the linear growth rate (or aggregation rate) increased from 3 to 8 nm/h at 115 °C when the water/silica ratio increased from 18 to 78. Van Grieken,[22] who used the same template/silica ratio (0.36) as that of Persson et al. (11,12), but at a water/silica ratio of 10.8 instead of 19.2, was able to produce smaller colloidal zeolite than that of Persson et al.[11,12] at a higher reaction temperature (170 °C).

Additional evidence for the effect of the water/silica ratio can be found in the works of Kirschhock,[23−25] in which they proposed a 33-mer and the so-called "nanoslab" as the precursor units obtained from 1 SiO_2/4 EtOH/0.37 TPAOH/4 H_2O system at room temperature. Since the precursors were prepared by the direct hydrolysis of TEOS in a 40% aqueous solution of TPAOH, the water/silica ratio was determined by the TPAOH/silica ratio. Strangely, however, this low water recipe was never employed again in other works by the same group[26−29] as well as a different group[30] trying to confirm their claims. A possible reason may be the difficulty in hydrolyzing TEOS in such a low water recipe. In fact, Kirschhock had to add the required TEOS to the 40% TPAOH solution in steps, with a few to 40 min of stirring each time to hydrolyze the TEOS.

A third clue for the peculiar effect of low water/silica ratio came from our recent work[31] on the controlled humidity steaming of dried gels produced by the concentration of a hydrolyzed TEOS/TPAOH/H_2O sol. We found that when most of the water in the precursor sol was evacuated, the gel obtained could be converted to zeolite at a lower relative humidity than that required for surfactant precipitated products.

In this paper, we demonstrate that, by concentrating a typical batch composition to a SiO_2 content of more than 30 wt %, we were able to produce silicalite nanocrystals smaller than ~50 nm via the two-stage varying-temperature procedure within a day. This is far shorter than that required by the "rapid synthesis" claimed in the literature, on the order of several days.[21] It turned out that this simple modification was very effective in preventing the aggregation of precursor particles into colloidal zeolite, and the silicalite produced appeared as transparent and fully dispersible nonagglomerated nanocrystals.

Experimental Section

The clear precursor sols employed in this study were prepared from TEOS (tetraethyl orthosilicate, 99.9%) and TPAOH (tetrapropylammonium hydrate, 40 wt % aq), both as reagent grade obtained from Merck. TEOS was added to a mixture of TPAOH (40% aq) and DI water. After stirring at room temperature in a closed PP bottle for about 50 min, the two-phase mixture turned into a clear single-phase solution (pH = 11.5−12). The molar compositions were 1 SiO_2/4 EtOH/0.25 TPAOH/R H_2O, where R = 18 or 78.

Rotary evaporation was done at 80 °C in a 250 mL PFA round-bottom flask to remove ethanol and water. When R = 18, it took only 90 min to concentrate a 123.74 g recipe to 35.13 g of transparent viscous fluid with a pH value of 12.9. Assuming all the ethanol and some of the water were the only species removed during the concentration step, the viscous fluid had about 34.2% SiO_2, 28.9% TPAOH, and the balance water. This corresponds to a H_2O/SiO_2 molar ratio of 3.6, which is the lowest compared to all previous research reports. When R = 78, it took 115 min to concentrate 339.75 g of clear solution to 33.77 g, leaving a SiO_2 content of about 35.5%.

The concentrated precursor sol was then distributed to several sealed vials and aged at 80 °C for different durations and coded as (concentrated precursor) #nCP, where n denotes the run number. A few drops of the aged #nCP sol were diluted 10 times with water and evaluated by DLS analysis as well as by UV/vis spectroscopy. Another part of the aged #nCP sol was left open at room temperature for 3 days and converted to a transparent glassy gel for XRD and FTIR measurements.

TABLE 1: Results of DLS and Light Transmittance Measurements on Concentrated Precursor Sols after Aging at 80 °C for Different Times[a]

sample code	aging time (h)	Z_{av}[b] (nm)	count (kcps)	poly-dispersity	T (%) at 600 nm
#1CP	0	4.4	295.53	0.208	98.9
	3	5.2	454.86	0.231	98.3
	6	4.9	339.58	0.445	97.6
	12	6.4	143.00	0.274	97.4
	18	22	245.44	0.306	97.4
	20	38.5	322.07	0.441	96.1
	22	35.0	364.00	0.102	94.2
	24	36.8	242.61	0.262	92.0
	26	38.9	282.61	0.080	89.7
	28	42.3	454.33	0.116	84.4
	30	44.4	329.52	0.084	77.5
	32	44.2	374.06	0.046	76.0
	36	43.6	318.82	0.057	71.4
	48	44.0	310.58	0.089	70.6
#1′CP	0	5.1	420.8	0.240	98.6
	2	5.1	151.9	0.220	98.7
	6	5.1	146.9	0.201	98.7
	10	7.1	175.2	0.311	97.4
	18	27.9	449.6	0.261	94.6
	24	42.5	385.6	0.103	94.3

[a] Both sols were prepared with an initial $[H_2O]/[SiO_2]$ ratio of 18 and then concentrated to a SiO_2 content of 34.2 wt % (#1CP) and 32 wt % (#1′CP) before aging. The DLS and transmittance measurements were done after dilution to ~3.5 wt %. [b] Measured with Nano-ZS.

TABLE 2: Results of DLS and Light Transmittance Measurements on Nanocrystal Sols #1NC Produced by Subjecting 24 h Aged #1CP Sol Described in Table 1 to 175 °C Hydrothermal Reaction for Various Times[a]

sample code	hydrothermal time (min)	Z_{av}[b] (nm)	count (kcps)	poly-dispersity	T (%) at 600 nm
#1NC	15	45.6	64.4	0.1210	89.9
	30	45.7	124.1	0.0675	73.5
	90	45.7	222.1	0.0934	67.1

[a] The DLS and transmittance measurements were done after dilution to ~3.5 wt %. [b] Measured with ZetaSizer-3000.

The concentrated precursor remained clear if the aging time was less than 18 h, but a detectable bluish haze due to scattering was noticed after about 24 h. At this stage, the viscosity of the sol increased and turned into a particulate gel when left in the sealed vial. By "particulate gel", we are referring to a gel that can be reverted to a viscous sol upon shaking, suggesting the gelation was formed via physical instead of chemical interactions. After that, the viscosity decreased upon further aging.

The 24 h aged concentrated precursor was then split into four fractions and subjected to hydrothermal treatment at 175 °C in a Teflon-lined autoclave for 15−180 min. The heating was done in a preheated convection oven. The original translucent viscous sol segregated into white sediments with a slightly yellowish clear supernatant on top. Some ammonia odor was noticed, suggesting decomposition of the TPAOH. If the supernatant was decanted, the remaining sediments, coded as #1NC (for nanocrystals), could be redispersed easily in ethanol or water to form a transparent to translucent sol again. Water redispersed #1NC was subjected to DLS and transmittance measurements to obtain the results listed in Table 2, while the remaining sediments were dried at room temperature for 12 h before XRD and FTIR analysis.

TABLE 3: Results of DLS and Light Transmittance Measurements on Nanocrystal Sols Prepared from 175 °C Hydrothermal Reaction of #2CP Sols Aged at 80 °C for Different Times[a]

sample code	80 °C aging time (h)	dilution before HT	Z_{av}[b] (nm)	count (kcps)	poly-dispersity	T (%) at 600 nm
#2NC	0	N	97.6	138.3	0.039	colloid
	3	Y	69	322.2	0.178	12
	6	Y	59	329.6	0.151	17
	6	N	48	299.9	0.108	32
	12	Y	45	306.7	0.115	46
	18	Y	46	392.1	0.089	55
	24	Y	45	358.0	0.119	55
	24	N	40	59.5	0.341	5[c]

[a] The #2CP sol was prepared with an initial $[H_2O]/[SiO_2]$ ratio of 78 and concentrated to a SiO_2 content of 35.5 wt %. The hydrothermal reaction was done directly with the aged #2CP sol or after 10 times dilution with water. The DLS and transmittance measurements were done with ~3.5 wt % sol. [b] Measured with ZetaSizer-3000. [c] Measured at 35.5 wt %.

In the run started with $R = 78$ (#2NC), the hydrothermal reaction was done on concentrated precursor sols that were aged for different period as listed in Table 3, whether as is or after 10 times dilution with water, but always for 90 min. If the hydrothermal reaction was done after dilution, a bluish translucent sol was directly produced instead of the sediment. In this run, the hydrothermal product was separated into two fractions by centrifuge at 18 000 rpm for 30 min. The clear supernatant was carefully decanted, and the transparent solid was redispersed in distilled water with ultrasonic vibration. The washing procedures were repeated three times. The extracted zeolite nanocrystals, or #2NC, were dried at 80 °C for 1 h and subjected to further characterizations.

To study the zeolite yield and the reason for incomplete recovery, several more experiments were conducted. The procedures are summarized in Table 4, along with the DLS and the transmittance results. In runs 3 and 4, the concentrated sol was aged at 80 °C for ~24 h, diluted 10 times with water, and subjected to 175 °C hydrothermal reaction for 90 min. In run 5, part of the aged sol was hydrothermal treated without dilution, while another part was diluted with aqueous HF to a lower pH value and aged again or reacted hydrothermally. After DLS and transmittance measurements, all CP or NC sols produced were centrifuged at 18 000 rpm for 30 min to extract the solids. The transparent solid extracted was dried at 80 °C for 1 h before characterization. The particle size and transmittance of the supernatant were again measured. The water in the supernatant was then evaporated by heating at 80 °C for 1 h. The weight of the silica in the yellowish viscous residue was then determined from the TGA analysis.

For comparison, colloidal zeolites (CZ/25 and CZ/09) were also prepared by the direct hydrothermal reaction of precursor sol at 175 °C for 90 min immediately after hydrolysis without the concentration and aging step. The precursor sol for CZ/25 had a molar ratio of 1 SiO_2/4 EtOH/0.25 TPAOH/38 H_2O, while that for CZ/09 was 1 SiO_2/4 EtOH/0.09 TPAOH/88 H_2O/0.03 NaOH. The products were centrifuged and washed as before. Colloidal zeolites with average particle sizes of 340 and 610 nm were obtained for CZ/25 and CZ/09, respectively.

Characterization

The size of the nanocrystals produced after hydrothermal reaction was analyzed by a ZetaSizer-3000 dynamic light scattering (DLS) instrument (Malvern, 10 mW He−Ne laser and a fixed scattering angle of 90°). However, this instrument was unable to resolve particles smaller than 10 nm, and a more sensitive model, Nano-ZS (Malvern, 4 mW He−Ne laser and a fixed scattering angle of 173°) was employed to analyze the particle sizes in the aged concentrated precursor sols. All measurements, whether of the aged concentrated precursors, CP, or the nanocrystals, NC, produced after hydrothermal treatment, were made under a concentration of ~3.5 wt % SiO_2 and analyzed with the NNLS (nonnegative least-squares) analysis software provided with the equipment. The transparency of the precursor sol was examined with UV−vis spectroscopy (Jasco-V-530) at the same concentration.

Powder X-ray diffraction (XRD) patterns were measured on a Shimadzu LAB-X-6000 diffractometer using Cu Kα radiation from $2\theta = 1.5$ to 40 range at a scan speed of 2 deg/min and a step size of 0.04 deg. FT-IR spectra were measured using the KBr wafer technique (1% w/w) in a Jasco-410 FT-IR spectrometer. The spectra were recorded with a resolution of 2 cm^{-1} in transmittance mode from 400 to 4000 cm^{-1} and corrected for background. TGA analysis was conducted on a Perkin-Elmer TGA (TAC 7/DX) at a heating ramp of 5 °C/min and in an air flow of 50 cm^3/min. Nitrogen adsorption measurements were carried out at 77.4 K on a Micromeritics ASAP 2010 instrument. Morphology of the zeolite nanocrystals was examined with TEM (JEM-2010, 200 kV). TEM specimens were prepared by placing a drop of the diluted sol (0.0001−0.0003 g/g of ethanol) on a carbon-coated copper grid.

TABLE 4: Results of DLS and Light Transmittance Measurements on Runs 3−5 as Well as the Partition of SiO_2 in the Supernatant and Extract after 30 min Centrifuge at 18 000 rpm for the Evaluation of Extraction Efficiency[a]

sample code	Z_{av} (nm)	count (kcps)	polydispersity	T (%) at 600 nm	SiO_2 super./extract
#3CP	41.4[b]	89.1	0.111	88.7	61/39
supernatant	40.1[c]	269	0.147	95.5	
#3NC	44.0[b]	128.5	0.168	55.8	19/81
supernatant	42.7[c]	468	0.055	96	
#4CP	51.0[b]	415.7	0.074	95	34/66
#4NC	50.0[b] (52.0[c])	424 (392)	0.085 (0.055)		15/85
#5CP	37.3[c]	190	0.105	94.9	89/11
#5NC	39.0[b]	54.5	0.140	1.5[d]	15/85
#5CP-A	38.4[b]	51.2	0.182	89.6	83/17
#5NC-A	50.0[b]	225	0.108	55.5	20/80

[a] #3CP was prepared with an initial $[H_2O]/[SiO_2]$ of 18, concentrated to 32.5 wt % and aged at 80°C for 24 h, and then diluted to 3.25 wt %. It was then hydrothermal treated at 175 °C for 90 min to produce #3NC. #4CP was prepared with an initial $[H_2O]/[SiO_2]$ of 38, concentrated to 32.2 wt % and aged at 80°C for 23 h, and then diluted to 3.22 wt %. It was then hydrothermal treated at 200 °C for 6 h to produce #4NC. #5CP was produced with an initial $[H_2O]/[SiO_2]$ of 18, concentrated to 34.2 wt %, and aged at 80°C for 24 h. The aged CP sol (pH = 11.1) was directly hydrothermal treated at 175 °C for 90 min to produce #5NC (pH = 13.1) or diluted with $HF_{(aq)}$ to 6.7 wt % (pH = 10.8) and then either heated at 80 °C for 2 h to produce #5CP-A or hydrothermally treated at 175 °C for 90 min to produce #5NC-A. [b] From ZetaSizer-3000. [c] From Nano-ZS. [d] Measured at 34.2 wt %.

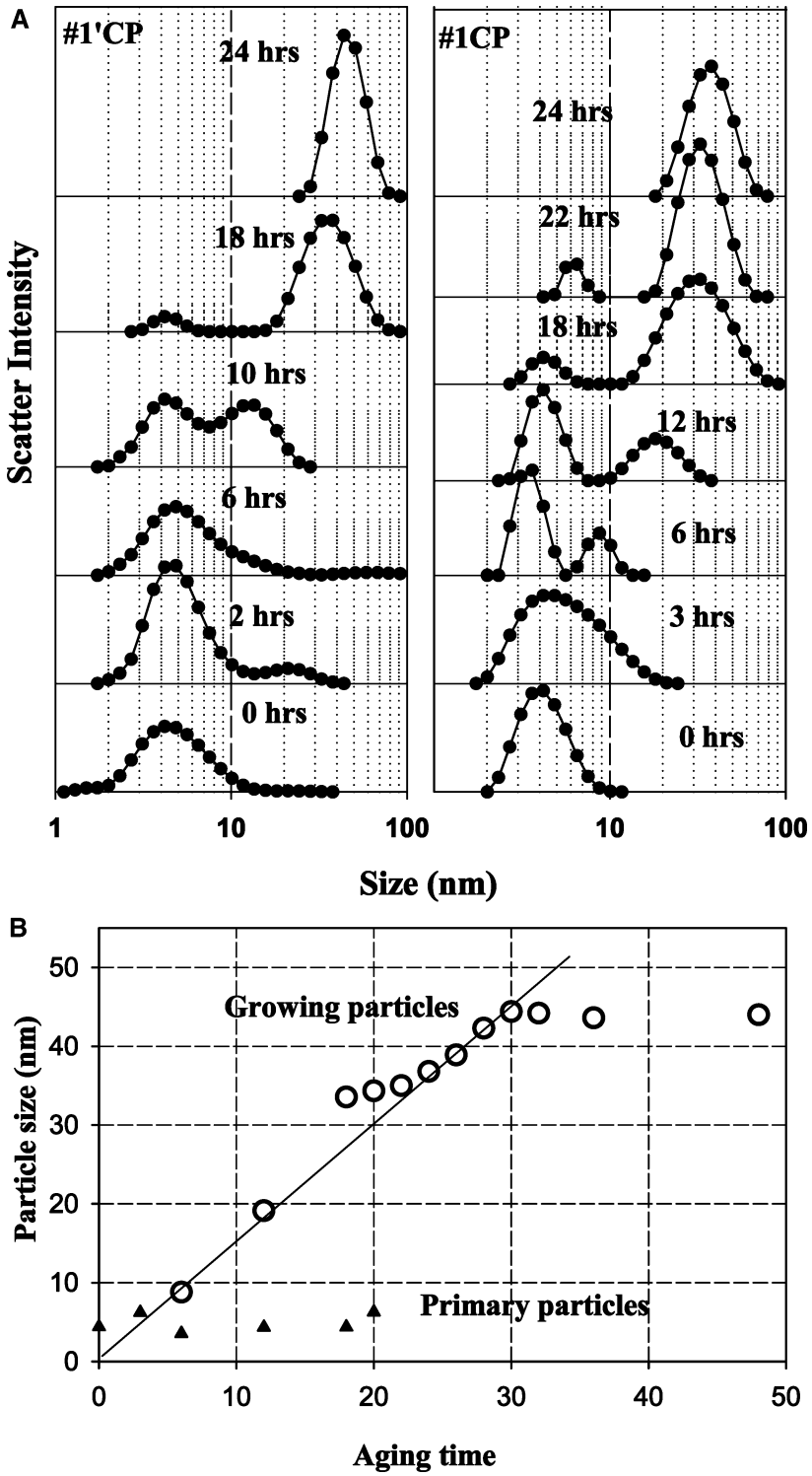

Figure 1. (A) Evolution of size distribution in the #1CP and #1′CP sols described in Table 1 after aging for the specified times at 80 °C. (B) Change of size with aging time for different populations. The sizes of the two populations were resolved by DLS analysis.

Results and Discussion

The results of the DLS and transmittance measurements are summarized in Tables 1−4. According to Table 1, the freshly concentrated precursor sol was a transparent viscous sol with transmittance ∼98% (diluted to 3.6 wt % SiO_2 at 600 nm). The transparency did not change much with aging until the noticeable haze appeared at ∼24 h, but the transmittance was still 92−94%. The transmittance decreased faster after that and reached a value of ∼70% for the 48 h aged sample.

The Aggregation Process during Aging. Despite the transparency, there were particles in the aged precursor sol. As listed in Table 1, the average size calculated from the DLS results increased with the aging time and reached a stable value after about 28 h. The change of particle size distribution during the 80 °C aging step is given in Figure 1A, where the results of two different runs with slightly different silica concentrations are presented. The general trend observed for these two runs was consistent. Subcolloidal particles with a broad size distribu-

tion centered at 3−5 nm were found in the freshly concentrated precursor sol, whose size remained about the same for 2−3 h of aging. A new population about 10 nm in size started to emerge after 6−10 h. This population grew to ∼30 nm after 18 h, along with a persistent population of the ∼5 nm subcolloidal particles. A final population centered at ∼45 nm was produced when the sol was well aged.

The existence of 3−5 nm subcolloidal primary particles in a clear TPAOH/TEOS/H_2O precursor sol has long been recognized.[32−35] Using simultaneous WAXS and SAXS, van Santen and co-workers[32] observed a persistent population of 2.8 nm primary particles and aggregates with diameters about 10 nm before the onset of crystallization at 125 °C. However, in their system, the crystallization process was associated with the consumption of the 10 nm aggregates and the formation of colloidal zeolite whose size depended on the alkalinity of the starting sol. There was a strong correlation between the number of crystals ultimately formed and the number of the 10 nm aggregates that appeared before crystallization.

It is interesting to note that the batch composition (1 SiO_2/0.244 TPAOH/*x* NaOH/11.4 H_2O) used by van Santen and co-workers had a similar TPAOH/SiO_2 ratio as ours and a water/silica ratio among the lowest compared to other studies. Extra sodium hydroxide was added to alter the alkalinity of the sol. As *x* increased, the concentration of the 10 nm aggregates decreased, and the onset of crystallization was delayed. At high alkalinity ($x = 1.24$), no 10 nm aggregates were observed. Without the addition of sodium hydroxide, the alkalinity in our case was not that high even after concentration. Thus, the formation of aggregates can be expected.

In an in situ light scattering study, Schoeman[14] demonstrated that, while aggregates formed and grew with time, the initial population of subcolloidal primary particles persisted for a long period of time. A plot similar to his is given in Figure 1B. However, unlike in his case, the size of the growing population quickly reached a plateau in our system. Furthermore, as will be demonstrated, the growing population did not become a zeolite until late in the process. That is, the system of particles grew in size, but not due to "zeolite crystal" growth.

A straight line fitted to the growing size estimated a growth rate of 1.5 nm/h. Compared to this, the value observed by Li et al.[18] at 80 °C with a sol about 9.7 wt % SiO_2 was 1.1 nm/h. The fact that a 3-fold increase of the initial silica concentration produced only 40% increase in the growth rate hints that the growth of the aggregates was not limited by diffusion. The limited growth of the aggregates can therefore be attributed to the high silica concentration employed. More aggregates must have been nucleated initially, whose growth had consumed all primary units in the first 30 h, leaving no nutrients for further growth.

The XRD patterns of the room temperature dried gels obtained from #1CP and #2CP sols aged for various times are plotted in Figure 2. The freshly concentrated precursor #2CP, after room temperature drying, is characterized by a broad diffraction band at about 23−27° typical for amorphous silica and a noticeable low-angle peak at around 3°. The low-angle peak could be due to the scattering of the 3−5 nm primary units detected in the DLS measurement and is similar to the low-angle X-ray scattering reported by Kirschhock et al.[24] However, strong low-angle scattering was also observed in #1CP that was aged for 18, 24, and 26 h. Since the DLS results indicated that the sol contains mainly ∼40 nm aggregates by this time, the strong peak at ∼3°, corresponding to a *d* spacing of 3 nm, hints that there may be some internal order in the aggregates.

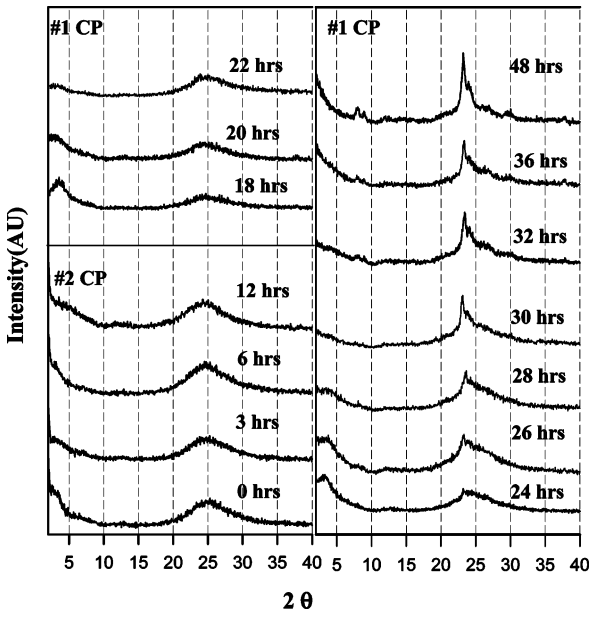

Figure 2. XRD patterns of the glassy solid obtained from #1CP and #2CP sols after aging for the specified time at 80 °C and drying at room temperature for 3 days.

As the aging time increased, a shift of the broad 23−27° silica diffraction band toward lower angles was noticed. The progressive downshift of the broad peak implies that the original amorphous silica has increasing resemblance to zeolite structure. A peak at 23°, which is the position of the major diffraction for silicalite, emerged in the 24 h aged sample. Above 32 h of aging, the characteristic diffraction at 7.9° and 8.8° for MFI structure also emerged. Note that the gradual transformation to zeolite is different from the result of Schoeman,[14] who had observed the characteristic peaks of MFI structure on the ∼10 nm particles centrifuged out from a rather young sample.

The gradual transformation to zeolite is consistent with the FTIR spectra displayed in Figure 3. In addition to the spectra of the samples discussed previously, that of the reference colloidal zeolite and nanocrystals produced after hydrothermal treatment also are given for comparison. In this figure, the bands at 1458, 1466, 1473, and 1489 cm^{-1} as well as the smaller peaks at 1559, 1540,1521, and 1507 cm^{-1} belong to the C−H bending modes of the TPA methyl groups. The band at 1388 cm^{-1} may be assigned to the CH_2 asymmetric wagging mode.[30] The most interesting part of the spectra is the siloxane (Si−O−Si) and silanol (Si−OH) stretch region from about 920 to 1250 cm^{-1}, respectively. As the aging time increases from 18 h toward 28 h and then to 48 h, the broad shoulder at 1220 cm^{-1}, typical for amorphous silica, gradually transformed into a distinct peak. At the same time, the large band originally at 1050 cm^{-1} also shifted gradually toward 1100 cm^{-1}. Both suggested the gradual formation of zeolite.

The spike at 970 cm^{-1} can be assigned to a localized Si−OH stretching mode. For amorphous silica, this would be a band at 950 cm^{-1}. However, because of the increase of polarity when Si−OH groups formed hydrogen bonds with TPA^+, particularly for TPA^+ enclosed in partially condensed silica cages, the stretching frequency increased and the band appeared as a sharp peak. By comparison, only a broadened hump was observed here for extracted nanocrystal #5NC-E and colloidal silicalite CZ/09, where most of the internal Si−OH groups had been eliminated.

The 750−850 cm^{-1} interval is related to the symmetric vibrations of the Si−O−Si bonds. For crystalline samples, only

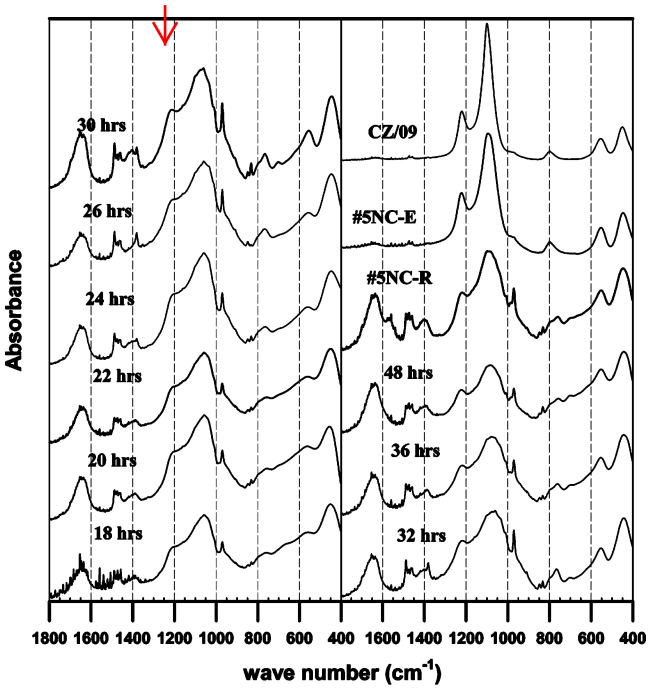

Figure 3. FTIR spectra of the glassy solid obtained from #1CP sols after aging for the specified time at 80 °C and drying at room temperature for 3 days. The spectra of #5NC and colloidal zeolite (CZ/09) are also shown for comparison, where #5NC-E and #5NC-R are respectively the extracted sediment and the residual silica in the supernatant after 18 000 rpm centrifuge for 30 min.

a band at 800 cm^{-1} was observed, but peaks at 847 cm^{-1} and a band at 760 cm^{-1} were seen in the spectra of the precursors. Finally, the modes in the 500−650 cm^{-1} region have been frequently assigned to the double 5-rings of silicalite. The younger precursor samples had only a broad band at ∼570 cm^{-1}. As the aging time increased, the corresponding band red-shifted toward 550 cm^{-1} and its intensity increased. The intensity reached a limit for precursors that had been aged for more than 30 h and remained the same even for colloidal zeolite.

Putting the above observations together, one concludes that the formation of the aggregates was the major event in the first ∼24 h of aging. The activity then shifted to the restructuring and densification (zeolitization) of the relatively amorphous aggregates already formed, leading to the progressive emergence of zeolite XRD peaks and IR characteristics. Another day of aging at 80 °C was needed to transform the aggregates into zeolite, and even then the yield was rather low, at about 60%. Although the formation, growth, and zeolitization of the aggregates happened in succession in this system, it is not yet clear whether the formation of aggregates is a prerequisite for subsequent zeolite formation.

Effect of Hydrothermal Reaction. To accelerate the transformation to zeolite, a higher temperature hydrothermal process after the formation of aggregates was advantageous. Knowing that the primary units are essentially depleted after ∼24 h of aging, this sol was directly subjected to hydrothermal reaction for different durations to identify the needed time.

As mentioned, white sediments were observed after hydrothermal reactions. The concentrated sol was highly alkaline, with a pH value of about 13. After hydrothermal reaction, the pH value increased even further, reaching a value of 13.6 if undiluted. It is known that the negative surface potential of zeolite nanocrystals maximized at pH ≈ 12.[36] The sedimentation of hydrothermal products must have occurred due to the high pH value. Upon dilution, the pH value dropped and the increased electrostatic potential became strong enough to disperse the nanocrystals. Table 2 showed that the transmittance of the diluted nanocrystal sols was not much different from the long aged precursor sol.

The XRD spectra of the #1NC nanocrystal samples obtained after hydrothermal reaction are shown in Figures 4A. Note that these samples were room temperature dried without centrifuge and thus contain as much weight of organics as that of silica. For the sample subjected to 15 min of hydrothermal treatment, this figure showed a shift of the original broad peak at ∼3° observed in 24 h aged #1CP toward higher angle, with a sharpened peak at 23°. For the 30 min treated sample, the 23° peak of zeolite clearly emerged, but the characteristic peaks at 7.9° and 8.8° were still missing. It took 90 min of hydrothermal treatment to bring about the full characteristics of the MFI structure. Beyond this point, further hydrothermal treatment, as exemplified by the XRD of 180 min treated sample, did not result in any noticeable changes in the XRD patterns.

To shorten the synthesis time even more, one can carry out the hydrothermal process before the depletion of primary units. As long as enough aggregates had already been nucleated, increasing the temperature would only accelerate their growth and zeolitization. However, if the hydrothermal reaction was conducted prematurely, the nucleation process may be altered. The total number of aggregates, and thus the final crystal size, would be different.

#2NC was therefore made by subjecting concentrated precursor sols that were aged for different durations to the same 90 min hydrothermal reaction. This time, however, the precursor sol was diluted 10 times with water, and the products were extracted and washed by centrifuge. For the diluted precursors, a translucent sol with bluish scattering was formed after the hydrothermal reaction. After centrifuging and washing, the extracted products remained redispersible in ethanol or water as long as the samples were not dehydrated. The transmittance of the redispersed nanocrystals varied from ∼12% to 55% and increased with the 80 °C aging time. This hints that the size of the nanocrystals produced changed with the aging time and was indeed confirmed by the DLS results listed in Table 3.

The extracted nanocrystals were dried at 80 °C for 1 h and subjected to XRD analysis. The obtained patterns are shown in Figure 4B. For #2NC obtained from 24 h aged CP sol, the peaks at 23−25° were overlapped, similar to that of nanocrystals obtained by hydrothermal reaction of 24 h aged #1CP for 90 or 180 min. The poor resolution of the XRD peaks was likely the result of peak broadening due to the very small crystal sizes. By comparison, the three peaks became increasingly distinguishable as the aging time before hydrothermal was shortened to 12 or 6 h, indicating increasingly larger crystal sizes.

The size distribution of the redispersed nanocrystals calculated from the DLS results has been plotted in Figure 5. As shown in this figure, colloidal crystals about 100 nm were produced from the hydrothermal reaction of unaged #2CP sol. The crystal size was reduced to 98, 69, 59, and then to 45 nm as the aging time increased from 0, 3, 6 to 12 h. If we assume all silica was converted to zeolite after hydrothermal reaction, the number density of crystals in the unaged and 3 h aged cases would be 4.6 and 1.6 times less than that in the 6 h aged case, respectively. In other words, the number of crystallization centers had increased 4.6 times during the 6 h of aging. Although there were no aggregates detected in the unaged or 3 h aged #2CP sol, the final product was still colloidal zeolites. If the aggregation of primary particles was a prerequisite for the formation of colloidal zeolites, it may have happened during the heating

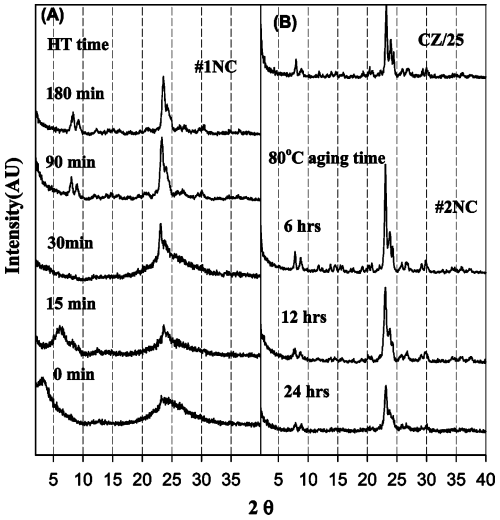

Figure 4. (A) XRD patterns of #1NC produced from 80 °C/24 h aged #1CP after 175 °C hydrothermal treatment for the specified time. (B) XRD patterns of centrifuged #2NC produced by 90 min/175 °C hydrothermal treatment of #2CP after aged for the specified time at 80 °C. The XRD pattern of colloidal zeolite (CZ/25) is also given for comparison.

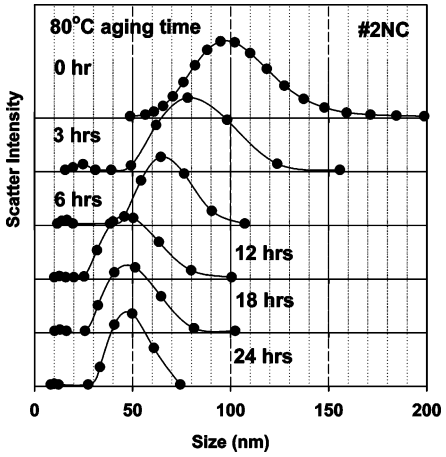

Figure 5. DLS size distributions of redispersed #2NC produced by 90 min/175 °C hydrothermal treatment of #2CP after aging for the specified time at 80 °C and diluting 10 times with water.

to 175 °C. Another possibility is that an undetectable amount of aggregates, or nucleation centers, had already formed during the 80 °C evaporation period and increased during the first 3 h of aging. This is very likely since a nonconcentrated precursor sol always produced much larger particles after 90 min of hydrothermal reaction at 175 °C. In any case, the size and number of aggregates in the CP sol seemed to reach a plateau when the aging time was extended beyond 12 h, as the final nanocrystal produced remained practically of the same size. In fact, it was observed that the size distribution of the nanocrystals was slightly sharpened due to Ostwald ripening, as the aging time before hydrothermal treatment increased from 12 to 24 h.

From the above results, it is clear that a fast process, with 12 h of aging at 80 °C and 90 min hydrothermal treatment at 175 °C, was sufficient to produce ~45 nm zeolite nanocrystals when a concentrated precursor was employed. The overall synthesis time required is only one-tenth that in previous reports. To highlight the difference of our approach, we have compared our results with that of Cundy et al.[20] in Figure 6. In their synthesis, the precursor sol was prepared with a recipe of 1 SiO_2/0.36 TPAOH/19.2 H_2O/4 EtOH. The clear sol was aged

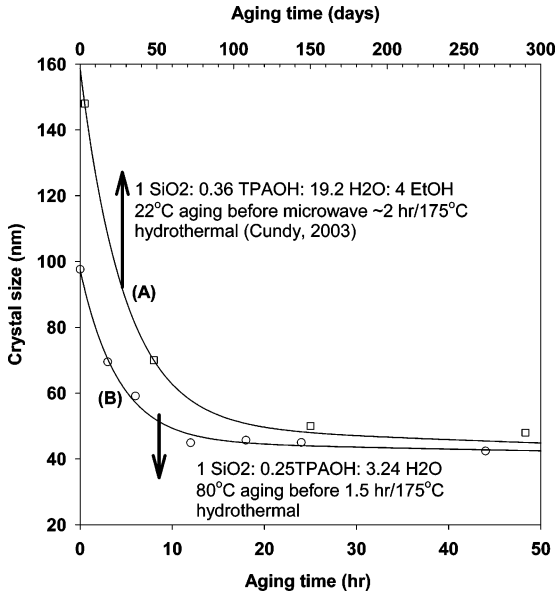

Figure 6. Comparison of the nanocrystal sizes produced via two-stage varying-temperature processes. (A) Results of Cundy et al.[20] with a recipe of 1 SiO_2:0.36 TPAOH:19.2 H_2O:4 EtOH. The clear sol was aged at 22 °C for several days and then subjected to a microwave heating at 175 °C for ~2 h. (B) This study; aging was done at 80 °C, followed by hydrothermal treatment at 175 °C for 1.5 h.

at 22 °C for days and then subjected to a microwave synthesis at 175 °C for ~2 h. Nanocrystals about 50 nm could only be produced after 150 days of aging. A similar exponential decay curve had been reported by Li et al.[18] on the same recipe using an aging temperature of 60 °C. The required aging time for producing ~50 nm nanocrystals was 150 h. In our case, ~50 nm nanocrystals were produced with just 12 h of aging.

In addition to the difference in the aging time scales, an interesting thing to note is the similarity of the limiting crystal size produced from the well-aged sols in all three cases. The unexpected consistency of the limiting size obtained from very different temperature and concentration conditions calls for further study. In any case, by concentrating the precursor sol, we were able to produce as many nucleation centers as Cundy et al.[20] and Li et al.[18] did, but in a much shorter aging time.

Characteristics of the Nanocrystals. It is known that a calcination temperature as high as 600 °C is needed to burn out the occluded template in micrometer-sized silicalite crystals. We reported[37] that the major decomposition of occluded TPA in silicalite nanocrystals happened at a lower temperature, although 550 °C was still needed to completely eliminate the silanols. This is consistent with what was observed in the TGA results presented in Figure 7A. For the ~600 nm colloidal zeolite CZ/09, there were two DTG peaks at ~400 and 450 °C, whereas the decomposition of TPAOH started at slightly higher than 300 °C and continued to above 500 °C in the case of 48 nm #2NC(6 h) produced by hydrothermal reaction of the #2CP sol aged 6 h without dilution. For the amorphous silica obtained directly from the 12 and 18 h aged #2CP sols, the major weight loss happened below 320 °C. There was a small but persistent weight loss as the temperature was increased to 600 °C. The 18 h aged sample was dried at 150 °C before subjected to TGA analysis; thus, the sharp DTG peak at 160 °C observed on the 12 h aged sample was absent. For these two CP samples, the weight loss between 170 and 320 °C must be associated with free TPAOH, which is known to decompose or evaporate at or below 200 °C. The delay of decomposition temperature to 320

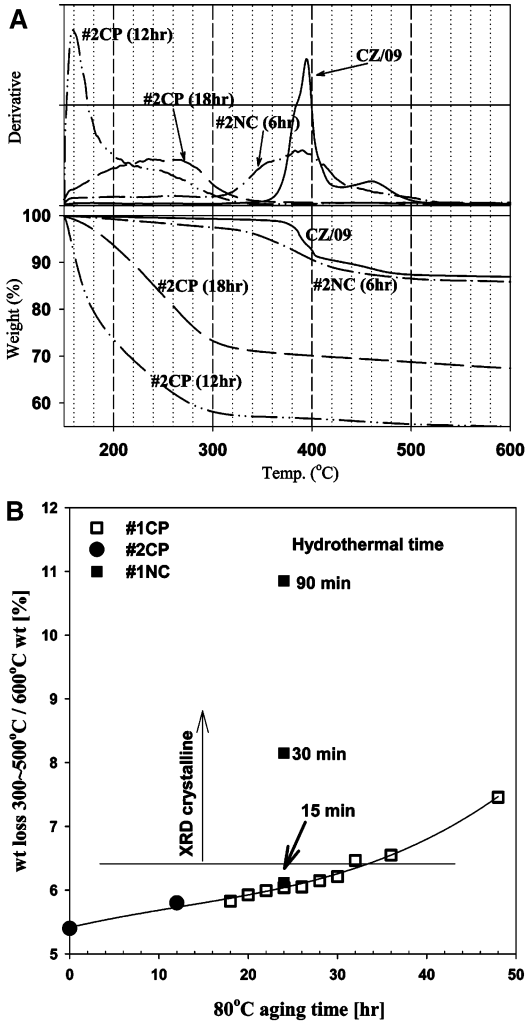

Figure 7. (A) TGA and DTA curves of #2CP aged at 80 °C for 12 and 18 h, #2NC produced from 6 h aged #2CP and colloidal zeolite CZ/09. (B) TGA weight loss between 300 and 500 °C relative to the remaining weight at 600 °C. Filled squares are for nanocrystals produced from 24 h aged #1CP sol after 175 °C hydrothermal reaction for the specified time.

°C could be due to the stabilization of some TPA^+ by surrounding silica.

On the basis of the above analysis, it seems appropriate to take the weight loss in the range of 300−500 °C relative to the remaining weight at 600 °C, as a measure of the amount of TPA confined within silica or as an estimate of the apparent MFI content in the sample. The results of such calculations are plotted in Figure 7B. It should be noted that the same calculation gave 13.4% and 13.7% for CZ/09 and CZ/25, respectively, while the value would be 13.0% based on four TPA^+ per unit cell of MFI. The data given in Figure 7B show that the apparent MFI content in the 80 °C aged CP sol increased with the aging time, and even the nonaged sample contained some confined TPA. That is, even the rotary evaporation step at 80 °C for 90−115 min was sufficient to precipitate a small amount of structured MFI. However, XRD crystallinity was only detected in samples showing more then 6.5% confined TPA. From the data corresponding to the #1NC samples hydrothermal treated for different durations, it is also clear that the majority of zeolite growth occurred only at the higher synthesis temperature of 175 °C.

The morphology of the nanocrystals produced is displayed in the TEM photographs shown in Figure 8. The low-

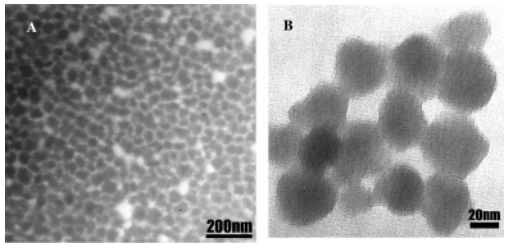

Figure 8. TEM picture of nanocrystals produced (a) extracted #2NC produced by 1.5 h/175 °C hydrothermal reaction of 12 h/80 °C aged #2CP sol and (b) extracted #4NC produced by 6 h/200 °C hydrothermal reaction of 23 h/80 °C aged #4CP sol.

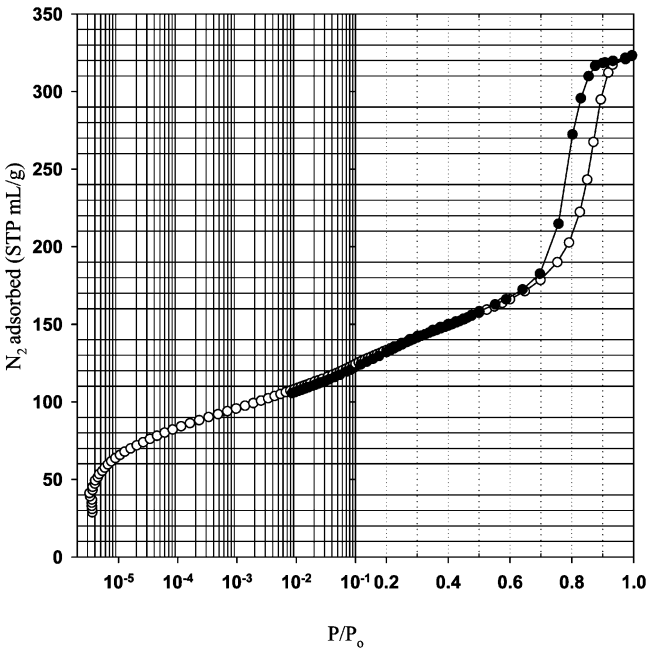

Figure 9. Nitrogen adsorption isotherm of extracted #2NC produced by 1.5 h/175 °C hydrothermal reaction of 24 h/80 °C aged #2CP sol. Open and solid symbols are for adsorption and desorption, respectively.

magnification picture demonstrates that the nanocrystals are fully dispersed, while the higher magnification picture shows that the nanocrystals were more or less spherical in shape. Although we were not able to see the lattice fringe of zeolites, the electron diffraction rings confirmed the particles are crystalline.

The nitrogen adsorption isotherm of centrifuged and washed zeolite nanocrystals produced from 90 min/175 °C hydrothermal reaction of 24h/80 °C aged #2CP sol is shown in Figure 9. To highlight the micropore volume filling, we have plotted the low-pressure part of the isotherm on a semilog scale. The TEM size of the particles in this sample was 40 nm. The BET surface area calculated from the isotherm is 460 m^2/g (fitted from 0.06 to 0.2 P/P_0), which is close to that of the S-20 sample synthesized at 60 °C for 10 days by Song et al.[6] Using the standard isotherm of Jaroneic,[38] we calculated an external surface area of 160 m^2/g, which is again consistent with the value Song et al. obtained from the difference of BET areas between uncalcined and calcined samples. The micropore volume calculated from our isotherm using the *t*-plot method was only 0.11 mL/g, which is about half compared to that of large silicalite crystals. However, Song et al. claimed that their S-20 sample was 20 nm in size by SEM and by Scherrer equation and argued that the measured surface area was consistent with the external surface area of 20 nm cubes. Our nanocrystals were ~40 nm in dimension, thus accounting for only half of the 160 m^2/g external surface area measured.

The difference in nanocrystal size estimated from adsorption data is again seen in the work of Aguado,[39] where our values on BET area, external area, and micropore volume would correspond to a crystal size of <20 nm (synthesized at 70 °C for 20 days or at 90 °C for 8 days) according to their Figure 8. One possibility could be that the spherical ~40 nm particles produced in our system were actually made of several crystallites of smaller size. This is consistent with the aggregation then local zeolitization sequence observed. However, the extra external surface area could also be attributed to the partially opened micropores at the crystal surface.

Zeolite Yield. Although we have demonstrated that silicalite nanocrystals could be made very rapidly from concentrated sols, the crystallinity and the yield were not discussed. In the conventional synthesis works, the crystallinity of zeolite is usually determined by the relative XRD peak height of the product comparing to micron-sized reference crystals. Such a practice will be invalid for nanocrystals, whose XRD peaks are affected by their small size.

The determination of crystal yield is also troublesome. The nanocrystals obtained are fully dispersible in water under alkaline condition and must be separated by high-speed centrifuge. The crystalline yield is thus significantly affected by the efficiency of the centrifuge process. In our case, the centrifuge was done at 18 000 rpm for 30 min, which may not be able to collect all the nanocrystals. For #2NC produced from undiluted 6 h aged CP sol, 92% of the silica was extracted by centrifuge. It was not clear whether the 8% loss corresponded to the dissolved fraction or loss of particles due to the inadequate centrifuge. Furthermore, it is important to clarify whether the semicrystalline nature of the 24 h aged precursor as displayed by its XRD pattern was the result of incomplete crystallization in all particles or the result of mixing crystalline with amorphous phases.

Thus, several more experiments were conducted, as summarized in Table 4, along with the DLS and the transmittance results. In all cases, the aged CP sols and the hydrothermal produced NC sols were centrifuged at 18 000 rpm for 30 min to extract the solid sediments. The supernatant collected was then evaporated at 80 °C for 1 h. The weight of the silica in the yellowish viscous residue obtained, as well as that in the extracted sediments, was obtained from the TGA results. The calculated partition of silica between supernatant and extract for different runs is listed in this table.

In this table, we find that a larger fraction, although still incomplete, of silica could be extracted by centrifuge from sols that had been hydrothermally treated compared to sol that was only aged at 80 °C. The more efficient extraction can be attributed to the higher density of the hydrothermal product compared to that of the aggregated produced by 80 °C aging. Nevertheless, a good fraction of the silica, having just slightly smaller size than that before centrifuge, remains in the supernatant. Comparing the results of runs 3 and 4, the extraction efficiency seemed to increase with the average size of the particles in the sol, suggesting that higher centrifuge force would further increase the extraction efficiency. On the other hand, higher solid concentration and the weaker surface potential also affect the extraction efficiency, as the same yield was obtained from the more concentrated, but smaller, crystals (#5NC) compared to the diluted, but larger, crystals (#4NC). In the same way, reducing the pH of the sol with acid seemed to hamper the extraction efficiency.

The extracted and the residual silica samples collected from experiment 5 were analyzed by XRD, and the results are shown in Figure 10. The extracted solid #5CP and #5CP-A were indeed crystalline. Although the main peaks overlapped, the 7.9° and 8.8° peaks were still noticeable. The crystallinity is better in the case of #5NC and #5NC-A. However, because fluorine was involved in the hydrothermal reaction leading to #5NC-A, the particle size obtained was larger than in the #5NC case. All residues collected from supernatants showed little crystallinity except in the case of #5NC. They are however different from a true amorphous silica. In fact, the IR spectra of extracted and residue parts of #5NC previously given in Figure 3 suggested that even the residue in the supernatant collected after centrifuge had as much crystallinity as the 48 h aged precursor. Therefore, for good crystallinity, a second step of high-temperature hydrothermal reaction is preferred. On the other hand, the XRD analysis does confirm that the aged precursor was not homogeneous as far as the crystallinity is concerned. Since the aggregates were rather uniform in their size, it seems that the onset of densification and zeolitization may have happened before the aggregates were fully grown.

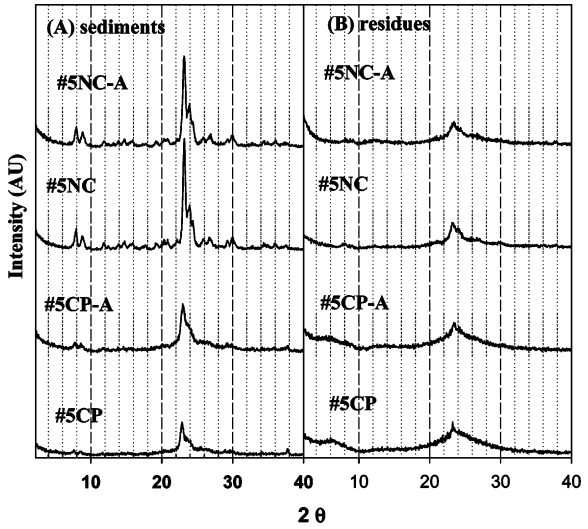

Figure 10. XRD patterns of (A) the solid sediments and (B) residues in the supernatant when the #5CP, #5CP-A, #5NC, and #5NC-A samples described in Table 4 were centrifuge at 18 000 rpm for 30 min. The suffix "-A" refers to acidification with HF.

A few more findings are worth mentioning here. As listed in Table 3, when the aged concentrated sol was hydrothermally treated directly without dilution, the final crystal size was slightly smaller than for the diluted case. For example, the direct hydrothermal treatment of 6 h aged #2CP sol produced nanocrystals of 48 nm compared to the 59 nm nanocrystals produced with the same sol after dilution, while the size decreased from 45 nm in the case of undiluted 24 h aged sol to 40 nm when this sol is diluted. The size of the nanocrystals produced in run 5, where the 24 h aged sol was not diluted before hydrothermal was also ~40 nm. Since the extraction efficiency was also higher with more concentrated product, the direct hydrothermal reaction of concentrated aged sol seems to be the preferred process for producing nanocrystals. Finally, a stability test had been conducted on a concentrated precursor sol that was aged for 17 h at 80 °C and left at room temperature for about a month. The DLS measurement showed Z_{av} of 35.3 nm with 0.125 polydispersity. Clearly, the 80 °C aged sol is very stable at room temperature, which may be of some practical interest.

It must be noted that concentrating the precursor sol by rotary evaporation was a rather troublesome step. Not only was it difficult to control the precise water ratio in the concentrated

sol, the uniformity of the product was also in doubt. A part of the viscous matter stuck to the bottle and seemed to be different from the fluid part. When the two fractions were separately aged at 80 °C for 6 h, their particle size distributions were somewhat different. This could have added to the broad size distribution observed in aged sols as well as the variation of the final crystal sizes.

The Crystallization Mechanism. The key difference in this approach to synthesize silicalite nanocrystals was the reduction of the water/silica ratio by evaporation prior to aging and hydrothermal treatment. The first occurrence of aggregation from the heating of a clear solution may not be too much different from more diluted systems. For example, for the 1SiO2/0.244TPAOH/*x*NaOH/11.4H_2O system employed by van Santen and co-workers,[32] the induction time at 125 °C, coinciding with the maximum scattered intensity from ~10 nm aggregates, was between 1 and 2 h. When a 0.25TPAOH/1TEOS/80H_2O sol was directly heated to 100 °C after hydrolysis,[37] the extrapolated induction time was about 4 h. With a recipe of 1SiO_2/0.36TPAOH/19.2H_2O/4EtOH and a reaction temperature of 80 °C, Li et al.[18] found the appearance of ~20 nm nanocrystals at ~25 h, which then grew linearly to 75 nm in 67 h. That we observed the formation of nanocrystals in 23 h is consistent with all the above results. The important difference in our case is that the nanocrystals did not grow after reaching ~40 nm and did not fully convert to zeolite until 48 h of aging at 80 °C.

The mechanism of forming silicalite-1 from a clear solution has been articulated by a number of reports[22,32,40] as beginning with the aggregation of primary units followed by the zeolitization (restructuring and densification) and growth of these aggregates. It is believed that the higher silica concentration we employed led to a faster and more complete aggregation of the primary units and consequently eliminated crystal growth during the later hydrothermal process. The silica concentration in our system is about ~5 times higher than that of Li et al.[16,18] Without considering other effects, the nucleation rate of the aggregates, which should be proportional to the square of the primary unit concentration, would be at least 20 times faster. Thus, most aggregates were nucleated within the first 12 h of aging, as supported by the size of the nanocrystals produced by hydrothermally treating the 12 h aged precursor. Between 12−30 h, the growth of the already formed aggregates dominates, but restructuring and densification of some particles cannot be ruled out. The available primary units were practically consumed at ~30 h, and the densification process continued at a slow pace.

If the formation of aggregates in the early stage of the aging process were the essential step for controlling the number of the growth centers and the final nanocrystals, we should be able to further reduce the crystal size by maximizing the number of aggregates formed. This seems to be unachievable yet. Despite the difference in recipes and aging temperatures, the ultimate crystal size that Cundy et al.[20] and Li et al.[18] obtained with well-aged precursor sol turned out to be similar to ours. More studies are required to fully understand this observation.

Conclusions

Our results are consistent with the previously proposed nucleation mechanism of silicalite-1 from a clear synthesis solution.[41] Primary TPA/SiO_2 units about 3−5 nm were present very early in the system. Upon heating, secondary aggregates started to appear, which eventually became zeolite nanocrystals via a restructuring and densification (zeolitization) process. If primary units remain in the system, further growth of the nanocrystals via addition the silica would be possible, either directly in the form of primary units or through the dissolution products of these primary units via an Ostwald ripening mechanism. By increasing the concentration of the synthesis sol, we were able to accelerate the formation of aggregates. The generation and growth of more aggregates quickly consumed most of the primary units in the system and set a limit to the size it can grow. Therefore, although the aggregates generated were initially larger than that observed previously in more dilute systems, the ultimate crystal size was slightly smaller. The overall effect was the acceleration of the synthesis rate for silicalite nanocrystals by more than a factor of 10.

Acknowledgment. We thank grants NSC93-2214-E-008-013 and NCU-ITRI 930103 from NSC of ROC and NCU-ITRI collaboration center, respectively, that made this research possible. We acknowledge the assistance of Prof. Ruaan with the DLS instrument. We also acknowledge the insightful comments on the first draft of this manuscript provided by Dr. Colin S. Cundy.

References and Notes

(1) Verduijn, J. P. Patent. No. WO 93/08125, 1993.
(2) Otterstedt, J. E.; Sterte, P. J.; Schoeman, B. J. Patent. No. WO 94/05597, 1994.
(3) Tosheva, L.; Valtchev, V. P. *Chem. Mater.* **2005**, *17*, 2494.
(4) Pu, S. B.; Inui, T. *Zeolites* **1996**, *17*, 334.
(5) Cundy, C. S.; Forrest, J. O. *Microporous Mesoporous Mater.* **2004**, *72*, 67.
(6) Song, W.; Justice, R. E.; Jones, C. A.; Grassian, V. H.; Larsen, S. C. *Langmuir* **2004**, *20*, 4696.
(7) Vilaseca, M.; Coronas, J.; Cirera, A.; Cornet, A.; Morante, J. R.; Santamaria, J. *Catal. Today* **2003**, *82*, 179.
(8) Sterte, P. J.; Hedlund, J.; Schoeman, B. J. Patent. No. US 6,177,373, 2001.
(9) Tsay, C. S.; Chiang, A. S. T. *AIChE J.* **2000**, *46*, 616.
(10) Larlus, O.; Mintova, S.; Valtchev, V.; Jean, B.; Metzger, T. H.; Bein, T. *Appl. Surf. Sci.* **2004**, *226*, 155.
(11) Persson, A. E.; Schoeman, B. J.; Sterte, J.; Otterstedt, J.-E. *Zeolites* **1994**, *14*, 557.
(12) Persson, A. E.; Schoeman, B. J.; Sterte, J.; Otterstedt, J. E. *Zeolites* **1995**, *15*, 611.
(13) Tsay, C. S.; Chiang, A. S. T. *Microporous Mesoporous Mater.* **1998**, *26*, 89.
(14) Schoeman, B. J. *Zeolites* **1997**, *18*, 97.
(15) Twomey, T. A. M.; Mackay, M.; Kuipers, H. P. C. E.; Thompson, R. W. *Zeolites* **1994**, *14*, 162.
(16) Li, Q. H.; Mihailova, B.; Creaser, D.; Sterte, J. *Microporous Mesoporous Mater.* **2001**, *43*, 51.
(17) Mintova, S.; Valtchev, V. *Microporous Mesoporous Mater.* **2002**, *55*, 171.
(18) Li, Q.; Creaser, D.; Sterte, J. *Microporous Mesoporous Mater.* **1999**, *31*, 141.
(19) Mintova, S.; Olson, N. H.; Senker, J.; Bein, T. *Angew. Chem., Int. Ed.* **2002**, *41*, 2558.
(20) Cundy, C. S.; Forrest, J. O.; Plaisted, R. J. *Microporous Mesoporous Mater.* **2003**, *66*, 143.
(21) Valtchev, V. P.; Faust, A. C.; Lezervant, J. *Microporous Mesoporous Mater.* **2004**, *68*, 91.
(22) Van Grieken, R.; Sotelo, J. L.; Menendez, J. M.; Melero, J. A. *Microporous Mesoporous Mater.* **2000**, *39*, 135.
(23) Kirschhock, C. E. A.; Ravishankar, R.; Verspeurt, F.; Grobet, P. J.; Jacobs, P. A.; Martens, J. A. *J. Phys. Chem. B* **1999**, *103*, 4965.
(24) Kirschhock, C. E. A.; Ravishankar, R.; Vanlooveren, L.; Jacobs, P. A.; Martens, J. A. *J. Phys. Chem. B* **1999**, *103*, 4972.
(25) Kirschhock, C. E. A.; Kremer, S. P. B.; Grobet, P. J.; Jacobs, P. A.; Martens, J. A. *J. Phys. Chem. B* **2002**, *106*, 4897.
(26) Kremer, S. P. B.; Kirschhock, C. E. A.; Aerts, A.; Villani, K.; Martens, J. A.; Lebedev, O. I.; Van Tendeloo, G. *Adv. Mater.* **2003**, *15*, 1705.
(27) Kremer, S. P. B.; Kirschhock, C. E. A.; Tielen, M.; Collignon, F.; Grobet, P. J.; Jacobs, P. A.; Martens, J. A. *Adv. Funct. Mater.* **2002**, *12*, 286.
(28) Ravishankar, R.; Kirschhock, C.; Schoeman, B. J.; Vanoppen, P.; Grobet, P. J.; Storck, S.; Maier, W. F.; Martens, J. A.; Deschryver, F. C.; Jacobs, P. A. *J. Phys. Chem. B* **1998**, *102*, 2633.

(29) Ravishankar, R.; Kirschhock, C. E. A.; Knopsgerrits, P. P.; Feijen, E. J. P.; Grobet, P. J.; Vanoppen, P.; Deschryver, F. C.; Miehe, G.; Fuess, H.; Schoeman, B. J.; Jacobs, P. A.; Martens, J. A. *J. Phys. Chem. B* **1999**, *103*, 4960.

(30) Kragten, D. D.; Fedeyko, J. M.; Sawant, K. R.; Rimer, J. D.; Vlachos, D. G.; Lobo, R. F.; Tsapatsis, M. *J. Phys. Chem. B* **2003**, *107*, 10006.

(31) Naik, S. P.; Chiang, A. S. T.; Thompson, R. W. *J. Phys. Chem. B* **2003**, *107*, 7006.

(32) de Moor, P. P. E. A.; Beelen, T. P. M.; van Santen, R. A. *J. Phys. Chem. B* **1999**, *103*, 1639.

(33) Ramanan, H.; Kokkoli, E.; Tsapatsis, M. *Angew. Chem., Int. Ed.* **2004**, *43*, 4558.

(34) Schoeman, B. J. *Microporous Mater.* **1997**, *9*, 267.

(35) Watson, J. N.; Brown, A. S.; Iton, L. E.; White, J. W. *J. Chem. Soc., Faraday Trans.* **1998**, *94*, 2181.

(36) Nikolakis, V.; Tsapatsis, M.; Vlachos, D. G. *Langmuir* **2003**, *19*, 4619.

(37) Naik, S. P.; Chen, J. C.; Chiang, A. S. T. *Microporous Mesoporous Mater.* **2002**, *54*, 293.

(38) Jaroniec, M.; Kruk, M.; Olivier, J. P. *Langmuir* **1999**, *15*, 5410.

(39) Aguado, J.; Serrano, D. P.; Escola, J. M.; Rodriguez, J. M. *Microporous Mesoporous Mater.* **2004**, *75*, 41.

(40) Kirschhock, C. E. A.; Ravishankar, R.; Jacobs, P. A.; Martens, J. A. *J. Phys. Chem. B* **1999**, *103*, 11021.

(41) de Moor, P. P. E. A.; Beelen, T. P. M.; van Santen, R. A.; Beck, L. W.; Davis, M. E. *J. Phys. Chem. B* **2000**, *104*, 7600.